

## Chandra Studies of Millisecond Pulsars in Globular Clusters

Jonathan E. Grindlay

*Harvard-Smithsonian Center for Astrophysics, 60 Garden St.,  
 Cambridge, MA 02138*

**Abstract.** The high resolution X-ray imaging and broad-band moderate resolution spectra enabled by the ACIS cameras on the Chandra X-ray Observatory have opened a new window in our study of millisecond pulsars (MSPs). Given the large excess of MSPs in globular clusters vs. the field, globular clusters are the favored sites for MSP study. Globular clusters (GCs) offer advantages of both known distance and likely MSP formation mechanisms but are complicated (or made more interesting!) by the complexities of subsequent MSP dynamical interactions. Here I review recent X-ray studies, focusing on our recent deep Chandra study of 47Tuc, which provide new constraints on both the spectra (thermal and non thermal) and evolution of MSPs and their encounters with both cluster and field stars.

### 1. Introduction and Overview

It is fitting that the oldest stellar systems in the Galaxy contain the oldest pulsars, the millisecond pulsars (MSPs), but not always in the oldest binary systems. Most MSPs in globular clusters (GCs) likely predate most of those in the field of the Galaxy given that the requisite neutron stars (NSs) in GCs were formed primarily from PopII massive stars which predated NS production from massive stars in the disk. At the same time, some of the MSPs in GCs (e.g. PSR B1821–24 in M28) are clearly younger, as evidenced by their spindown ages  $P/2\dot{P}$  (however approximate these may be). These suggest either recent spinup of old NSs, or more recent NS production from accretion induced collapse of white dwarfs in cluster binaries, or possibly  $\dot{P}$  values enhanced by mass transfer in a retrograde second exchange of an old MSP (see below). In fact it has become clear that some MSPs in GCs (e.g. 47TucW; discussed in more detail below) have had at least one swapped binary partner and thus more complex histories than any in the field.

New clues into the nature, formation and evolution of MSPs have come from the additional constraints that  $\sim 0.3\text{--}8\text{ keV}$  X-ray observations of their integrated or pulsed emission provide. The high sensitivity, spectral resolution and bandwidth of the Chandra and XMM-Newton X-ray Observatories have enabled great progress in studies of MSPs. The great increase in angular resolution with Chandra has been essential for studies of MSPs in crowded GC cores. The first moderately deep Chandra observation of 47Tuc (Grindlay et al. 2001a; hereafter GHE01) provided a dramatic view of GC-MSPs and enabled (via X-ray to optical boresites) the optical identification, with HST, of the first MSPs in globulars. Accordingly, in this review we shall focus on Chandra (and some

HST) results and only discuss briefly some recent XMM (and earlier ROSAT) studies.

The first optical identifications of MSPs in GCs, two in 47Tuc (Edmonds et al. 2001, 2002) and one in NGC 6397 (Ferraro et al. 2001), have provided direct evidence that some GC-MSPs have swapped their binary partners. The main sequence or somewhat evolved binary companions now found in two such systems (PSR J1740–5340 in NGC 6397 and MSP W in 47Tuc, as discussed below) are not expected for systems that have evolved directly from their parent LMXBs. Post-LMXB secondaries are He white dwarfs (He-WDs) or very low mass degenerate remnants in field MSPs and most GC-MSPs. The nature and evolution of both of these systems is further constrained by their X-ray spectra and variability. The recently derived spectrum for MSP W in 47Tuc (hereafter either 47TucW or MSP W) shows hard emission, possibly from gas near the L1 point shocked by the pulsar wind (Bogdanov, Grindlay and van den Berg 2004, hereafter BGvdB04) and similar to that reported (Grindlay et al. 2001b, Grindlay et al. 2002; hereafter GCH02) for the Chandra source and MSP in NGC 6397, PSR J1740–5340 (hereafter 6397A). Even more important is that the spectra, luminosity and X-ray vs. optical variability of 47TucW show remarkable similarities to the accreting MSP J1808.4–3658, thus providing the crucial missing link between radio MSPs and LMXBs (BGvdB04).

Recent Chandra studies of MSPs in GCs, as reviewed here, have now established that MSPs can show three different spectral components: very hard non-thermal emission (magnetospheric; with power law photon index  $\sim 1$ ) vs. hard (with PL index  $\sim 1.5$  and probably due to shocked gas) vs. soft (thermal emission from the NS polar caps, with typical  $kT \sim 0.1$  keV). In this review we focus on the hard and soft components. Whereas both the very hard magnetospheric and soft thermal (polar cap) emission were evident from ROSAT spectra and timing (cf. Becker and Trumper 1999), the Chandra detection of the shocked gas component has required the high resolution imaging of Chandra to both isolate the source from neighbors and to enable HST identification of a heated stellar companion as the likely source of gas. It has also required sufficient temporal coverage to establish spectral variation with binary phase (for 47TucW). Although pulsation spectra and pulsed light curves are also both highly desirable, spectra are arguably more important for a first investigation of MSP properties and have meant that the ACIS (with  $\sim 150$ – $200$  eV resolution), rather than the HRC (with virtually no energy resolution), Chandra cameras have been used in most GC-MSPs studies to date. Thus pulse-phased spectra for multiple MSPs imaged with Chandra are not possible (although this could be done in principle for a single MSP observed with the LETG grating and HRC-S), and HRC-S imaging pulsed light curves are only available for one MSP (J0437–4715, in the field; Zavlin et al. 2002). As discussed by BGH04, such “grey” pulsed light curves can constrain MSP emission and neutron star properties.

## 2. Brief Overview of X-ray Studies of MSPs in Globular Clusters

### 2.1. The Brightest and Hardest

The X-ray brightest MSP in a globular cluster is the source in M28, PSR B1821–24, first detected and resolved with the ROSAT HRI (Danner et al. 1997) and for which high quality spectra (but with no temporal resolution for pulsations) have been obtained with Chandra (Becker et al. 2003). If this were the only MSP studied in X-rays, our view of their properties would be very different: its predominantly non-thermal emission and narrow pulse profile in X-rays is very different from that now inferred (GCH02, Bogdanov et al. 2004, hereafter BGH04) for the bulk of the MSP population in 47Tuc with their predominantly thermal spectra (GCH02). Unambiguous X-ray spectra for even this apparently brightest GC-MSP require the spatial resolution of Chandra, given source confusion (Becker et al. 2003), although RXTE hard X-ray spectra for the (narrow) pulse peak (Kawai and Saito 1999) are in reasonable agreement.

Upper limits have been obtained with RXTE for hard X-ray emission from the integrated population of MSPs in 47Tuc (Ferguson et al. 1999), and RXTE has been able to provide spectra and timing constraints on the brightest nearby MSPs in the field. At  $\gamma$ -ray energies, the very flat non-thermal spectrum (with photon index  $\sim 1$ ) is detectable for B1821–24 and may have been detected with EGRET (cf. Zhang and Cheng 2003). MSPs in the field, which are generally much closer than the GC-MSPs, have been detected at  $\gamma$ -ray energies (e.g. J0218+4232, detected convincingly with EGRET by Kuiper et al. 1998). Its broad soft X-ray pulsed light curve suggests a thermal component, confirmed by its combined thermal plus PL spectrum detected with XMM-Newton (Webb, Olive & Barret 2004). Detection of the non-thermal components of nearby thermally-dominated MSPs in the field (e.g. J0437–4715) may constrain the evolution of the magnetospheric spectra with the B field at the light cylinder, which may be correlated with non-thermal X-ray luminosity, as shown below.

### 2.2. vs. the Dim and the Soft

As suggested above, most MSPs in GCs are not bright and hard; B1821–24 is the exception. Rather, as our initial studies of the MSPs in 47Tuc have shown (GHE01, GCH02), the norm is relatively low X-ray luminosity, primarily in thermal emission and distributed in a relatively narrow band:  $\sim 2\text{--}8 \times 10^{30}$  erg s $^{-1}$ . This was not apparent to ROSAT and the pioneering studies, and review, of Becker and Trumper (1999) since again the samples were dominated by nearby or by extreme objects. The virtue of the GC-MSPs is, again, that they can define MSP parameters for entire populations in a single observation, given (of course) the required angular resolution and sensitivity.

This population-view, afforded by Chandra, can not only define the role of MSPs in binary evolution and thus cluster evolution, but in MSP or NS evolution as well. One of the key questions posed in GCH02 was: if MSPs are indeed swapping partners, as evidenced by 6397A or 47TucW (see below), then what must be the fate of i) the  $P$  and  $\dot{P}$  history, if matter accretes with randomly aligned angular momentum vector  $\mathbf{J}$  from the new secondary onto the “old” MSP during the re-exchange, and ii) the  $B$  field, both surface and at the light cylinder, if  $B$  field evolution on NSs has anything to do with the accretion

history of the star, as is commonly believed? We address some of these issues here and in more detail in forthcoming journal papers.

### 2.3. From Hard to Soft (and back)?

As shown below, the hard-bright MSPs have young ages ( $P/2\dot{P}$ ) vs. the opposite for the dim-soft (reminiscent of other aging populations!). Does re-recycling restore youth? If so, could some of the apparently young MSPs (e.g. B1821–24) be masquerading youth after re-spinup in a second exchange, as the  $B$  field is amplified by the differential rotation between a newly-accreted outer layer that is misaligned with the original  $\mathbf{J}$  and  $\mathbf{B}$  vectors? Or, more likely, is its NS a relic of the cluster formation and been able to maintain its stronger  $B$  field without internally driven decay until its recent first-time accretion episode when it was exchanged in a binary encounter to acquire its first partner?

On the other hand, the soft-dim MSPs, like those which predominate in 47Tuc, may be resurrected (as for MSP W) with a “new” main sequence companion apparently heated by the pulsar wind to produce mass loss through L1 that in turn is shocked by the pulsar wind to produce hard X-ray emission. This renewed hard emission phase for an MSP would be characterized by a lack of hard X-ray pulsations, though soft and sinusoidal pulsations are still expected from the polar caps. Resurrected MSPs would likely show a smooth modulation with binary phase if (as for 47TucW) part or all of the shocked-gas emission region is eclipsed by the companion. Such a doubly-recycled MSP can thus be hard but old (both chronologically and as measured by its new  $P/2\dot{P}$ ). On the other hand, given the bizarre torques that must occur when a randomly aligned “old” MSP exchanges its (usually) degenerate secondary for a main sequence star and then has renewed mass transfer and spinup, the *deceleration* accretion torque from a retrograde second capture could cause the  $P/2\dot{P}$  age to appear young despite a previously reduced  $B$  field.

These are representative questions raised by the fascinating demography of GC-MSPs. Let us look again at the MSP population in 47Tuc, but now with the additional perspective of a much deeper Chandra observation.

## 3. Chandra Probes Deeper into 47Tuc

Over a 13 day interval (September 29 – October 11, 2002, we observed 47Tuc with four 65 ksec ACIS-S pointings and matched short (5ksec) sub-array exposures (to deal with bright sources). Simultaneous HST/ACS images were obtained in three filters (B, R and  $H\alpha$ ) for 3 HST orbits on each of Chandra observations 2 – 4. This Large Chandra Program was motivated in part by the MSP population, detected for the first time as soft X-ray sources with the less sensitive (at low energies) ACIS-I imager in our single 70ksec observation in March 2000 (GHE01). The overall source catalog for the ACIS-S observations is reported by Heinke et al. (2004a): some 300 sources are detected within the cluster half-mass radius of  $2.8'$ . In Figure 1 we show a representative color image constructed from the summed exposures in the 0.3–1.2 keV (red), 1.2–2 keV (green) and 2–6 keV (blue) bands.

All 16 MSPs located with timing positions (Freire et al. 2001), and 47TucW which was identified by the discovery (Edmonds et al. 2002) of its optical coun-

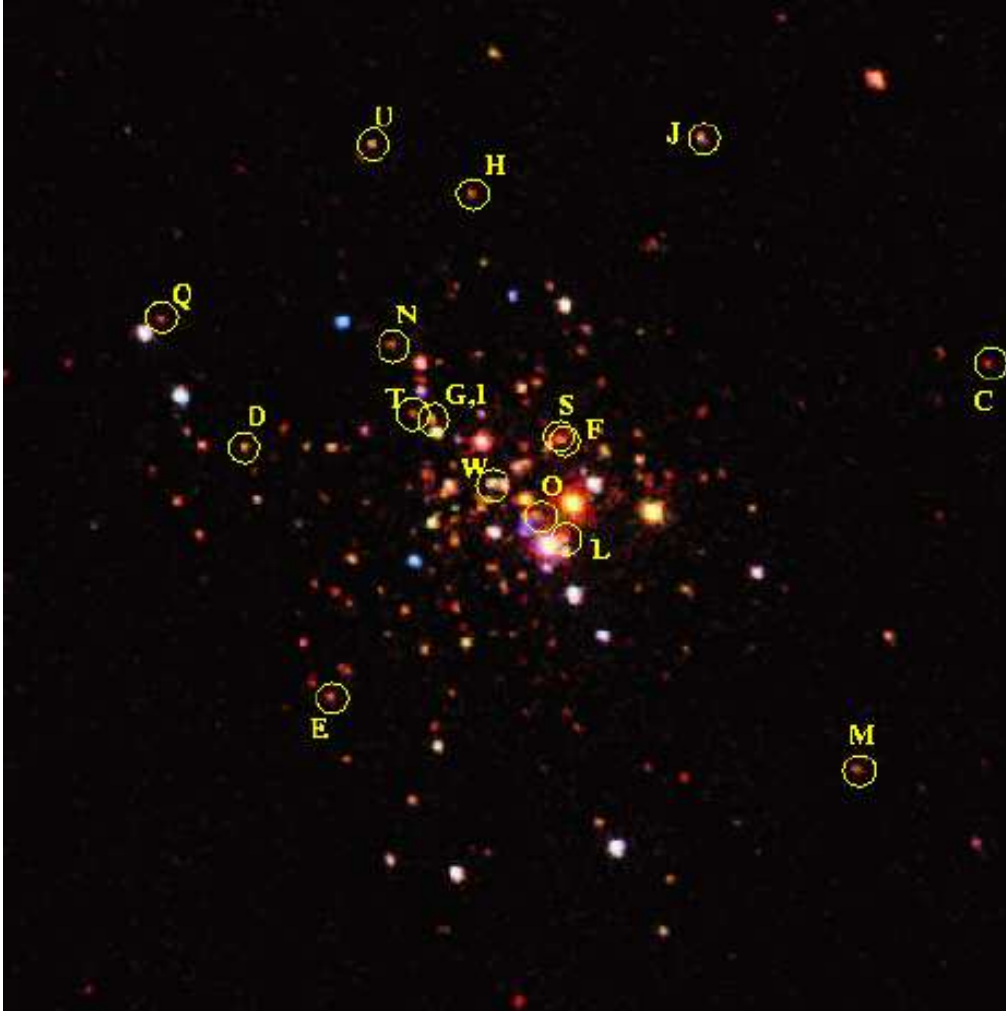


Figure 1. Representative color image (from Heinke et al. 2004a) of central  $2.5' \times 2.5'$  of the deep ACIS-S exposure (270 ksec) on 47Tuc, with all 17 MSPs with known locations detected as marked. MSPs F and S, separated by  $0.74''$ , are partially resolved but G and I, separated by  $0.12''$ , are not. The Chandra positions are much more accurate than the large circles shown, with rms deviation from the MSP positions of only  $\sim 0.2''$ . (NOTE: this image compressed for astro-ph size limits; original to appear elsewhere.)

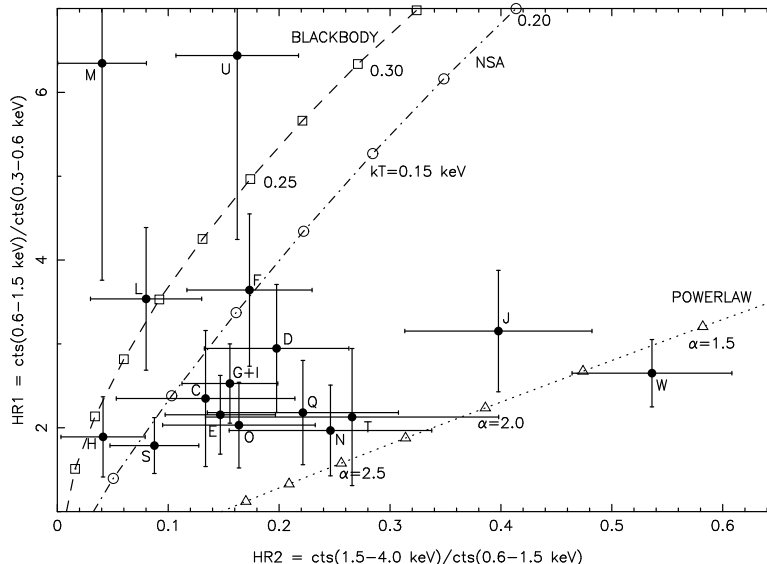


Figure 2. X-ray color-color diagram for the MSPs in 47Tuc (from Bogdanov et al. 2004) vs. model tracks folded through the detector for fixed cluster column density  $N_H$  and blackbody emission or neutron star atmosphere (NSA) temperatures, or power law spectra with photon index values shown.

terpart with photometric periodicity and phase identical to the radio values, are clearly detected (though G and I, with  $0.12''$  separation, are not resolved) in this deep Chandra image. Several MSPs, particularly C and T, were marginal detections in the original ACIS-I image but are now well detected. The total counts recorded in the summed Chandra images for each MSP range from 38–306 over the 0.3–4 keV band. This has allowed new studies (Bogdanov et al. 2004, hereafter BGH04) of the spectra and variability of this largest MSP sample in a single GC. We preview several key results from this work and provide some additional constraints on the X-ray spectra and properties of MSPs.

### 3.1. Colors, Spectra and Luminosities of MSPs in 47Tuc

First, the  $\gtrsim 5\times$  better count statistics as well as improved soft response of ACIS-S (despite its low energy degradation with time) allow the X-ray colors and thus spectral characteristics of even the faintest sources to be better determined. Figure 2 shows the color-color diagram, derived in softer bands appropriate for ACIS-S, and comparison of the MSPs with tracks for blackbody (BB), neutron star atmosphere (NSA; Lloyd 2003) and power law (PL) models derived for the ACIS-S response and latest measurement (Gratton et al. 2003) of the cluster reddening from which we derive  $N_H = 1.3 \times 10^{20} \text{ cm}^{-2}$  (Heinke et al. 2004a). Whereas the ACIS-I color-color plot, with larger errors, suggested that all but MSP J (MSP W was not yet identified) were consistent with pure thermal emission (GCH02), Figure 2 suggests that most MSPs are a mixture of thermal and power law models, or possibly a two temperature thermal model and additional hard component, as derived by Zavlin et al. (2002) for the field MSP J0437–4715.

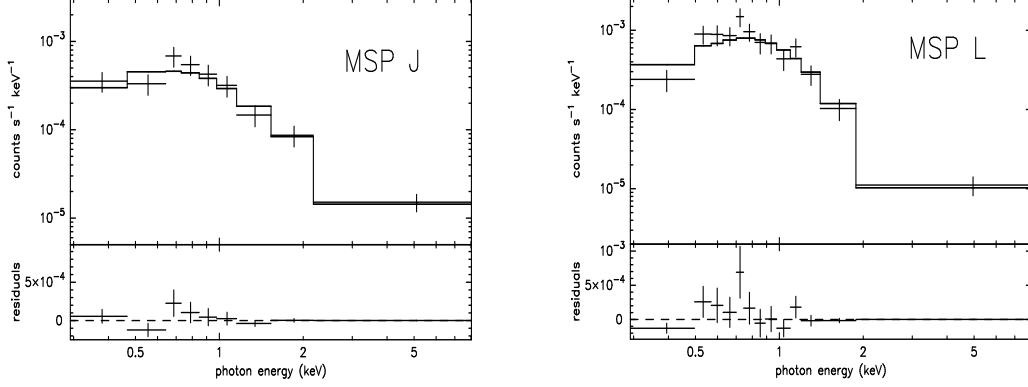


Figure 3. Spectral fits (Bogdanov et al. 2004) for two MSPs bright enough to clearly require hard spectral components in addition to a soft thermal component. MSPs O and, especially, W also require such a two-component model. The fits shown here are for a NSA + PL model but are fitted for NSA temperature only with PL photon index  $\Gamma = 1$  and  $NH = 1.3 \times 10^{20} \text{ cm}^{-2}$  held fixed. The derived NSA temperature  $T(10^6 \text{ K})$  and radius  $R(\text{km})$  values,  $(T, R)$ , for J and L are  $(0.89 \pm 0.18, 1.59 \pm 0.76)$  and  $(1.25 \pm 0.16, 1.07 \pm 0.30)$ .

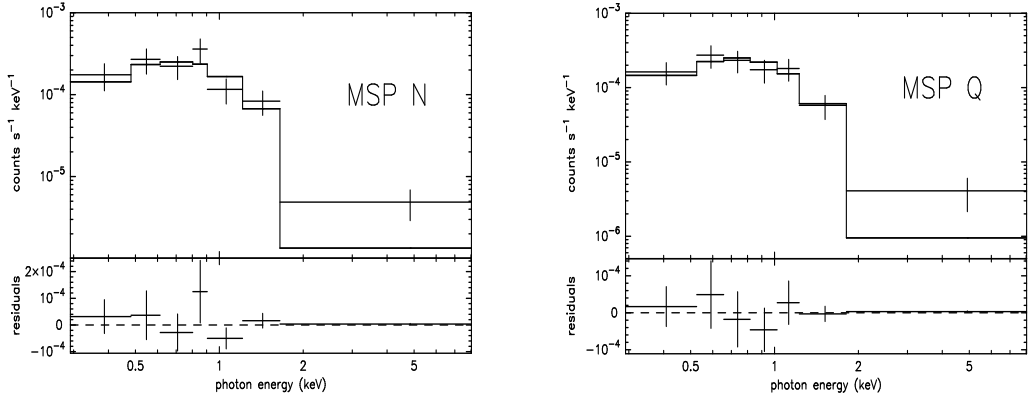


Figure 4. Spectral fits (single temperature NSA model only; from Bogdanov et al. (2004)) vs. data for fainter MSPs showing excess flux above NSA model in highest energy bin.

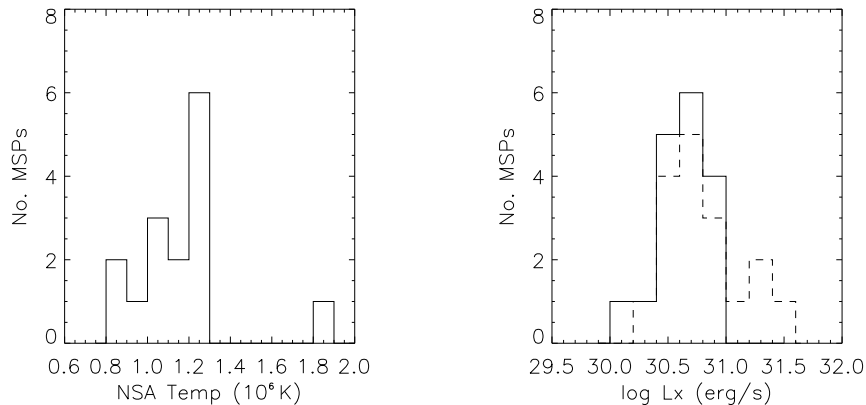


Figure 5. a) Left, temperature distribution for NSA model fits to MSPs in 47Tuc; b) Right, thermal luminosity distribution (solid histogram) derived from  $R$ ,  $T$  values from NSA model fits vs. X-ray luminosity derived from total flux in 0.01–8 keV band (dashed histogram; see text). The non-thermal (PL?) luminosity may be estimated from the difference between the total and thermal components.

The improved statistics now allow direct spectral fits for NSA models (BB fits, with larger  $kT$  but smaller radii, are equally acceptable) and an additional PL component. Spectral fits were done by requiring at least 15 counts (or 10 counts for the faintest MSPs) per spectral bin and were thus limited by statistics: the highest energy bins included in the fit exceeded 2 keV only for the brightest-hardest 4 MSPs: J, L, O and W. Spectral fits for these four were done for a NSA + PL model by holding the photon index fixed at 1 for the PL component. Only MSP W was bright enough to fit the NSA and PL components separately, giving a photon index  $\Gamma = 1.3 \pm 0.2$ . Spectra are shown in Figure 3.

For the remaining 11 MSPs (the unresolved and partly resolved MSP pairs, G+I and F+S, were each fitted as if one object), the fits were done for an NSA model only. However these typically showed an excess above the soft NSA fit at energies above 2 keV, as shown in Figure 4 for MSPs N and Q. Thus we now conclude that although the soft-thermal emission is dominant, it is likely that most of the 47Tuc MSPs also contain an underlying harder component. It is interesting then to examine these thermal and hard components separately.

### 3.2. Spectral properties vs. MSP properties

The distribution of thermal temperatures, for an assumed neutron star atmosphere (NSA) model (we use the Lloyd (2003) model), is surprisingly narrow as shown in Figure 5a. All of the MSPs have their thermal emission fit by NSA models with mean temperatures (in units of  $10^6$  K)  $T_6 = 1.18 \pm 0.22$ . In fact *all* of the MSPs except U, with  $T_6 = 1.83$ , have their polar cap temperatures within the narrow range of  $0.9\text{--}1.3 \times 10^6$  K. This presumably reflects a nearly constant heating rate, despite the  $\gtrsim 10\times$  range of MSP ages.



The fitted polar cap radii are also relatively narrowly distributed, with mean value  $R = 0.91 \pm 0.46$  km, and – given the NSA model – is larger than the BB radii discussed in GCH02 as evidence the  $B$  fields may be multipolar. The corresponding thermal emission luminosity, derived from a Stefan-Boltzmann application of the NSA-derived  $R$ ,  $T$  values, is shown in Figure 5b. We have assumed the thermal emission is from two polar caps, each of radius  $R$  (both  $R$  and  $T$  are evaluated at the NS surface), and have approximated their combined luminosity as  $2\pi R^2 \sigma T^4$ , where  $\sigma$  is the Stefan-Boltzmann constant. This is an approximate upper limit since it ignores the unknown projection effects of the polar caps due to the  $B$  field inclination, and also ignores the exact effects of gravitational bending near the NS. While exact photon bending corrections are not known, they nevertheless ensure that both caps are seen at least partly. The thermal luminosity distribution (solid curve) has mean value  $\log L_{\text{thermal}} = 30.64 \pm 0.25$  whereas the luminosity derived from integrating the total flux in the 0.01–8 keV band (dashed histogram) has mean  $\log L_{\text{tot}} = 30.80 \pm 0.32$ . The latter luminosity was derived from the detected counts over this band for the two-component model (NSA + PL) spectral fits derived over the 0.3–8 keV band and then integrated over the broad band (0.01–8 keV) in XSPEC for an estimate of the total flux.

The fact that the MSP spectra can be decomposed into thermal and total components (Fig. 5b) suggests that the underlying hard component (here approximated by a PL) might be extracted by simple subtraction. If this hard component is indeed non-thermal and a PL, then this would allow constraints on the evolution of this magnetospheric emission vs. fundamental MSP properties such as magnetic field or age. In Figure 6 we show the possible dependence of the hard luminosity component (i.e. the excess above the NSA thermal flux) on a) magnetic field at the MSP light cylinder,  $B_{\text{lc}}$ , and b) the dependence of this same hard luminosity of spindown age. The intrinsic  $\dot{P}$  values required for either  $B_{\text{lc}}$  or  $P/2\dot{P}$  are corrected for cluster acceleration as derived in GCH02. The MSPs display a weak (85% confidence level from a Spearman rank correlation) correlation between the PL luminosity,  $L_{\text{PL}}$ , and magnetic field at the light cylinder,  $B_{\text{lc}}$ , and suggest a possible anti-correlation between  $L_{\text{PL}}$  and spindown age. Both correlations are suggested by the data presented in GCH02 and Bogdanov et al. (2004) but are more apparent in the attempted decomposition of the PL or hard luminosity presented here.

Note that this “PL Luminosity” may not be magnetospheric non-thermal emission, though this is plausibly at least partly the case. Instead, some MSPs could have their hard component due to their pulsar winds shock heating gas driven off from their binary companions, as is the case for MSP W (BGvdB04). At first this seems unlikely since none of the MSPs in Figure 6 have binary mass functions and constraints on inclination (e.g. eclipses) which require main sequence companions as is the case for MSP W. Freire (2004, in this volume) discusses the distinction between the low mass binary pulsars (LMBPs), for which mass functions require secondaries with masses  $\gtrsim 0.1 M_{\odot}$  and which are usually He white dwarfs, and the eclipsing LMBPs (ELMBPs) such as MSP W for which the main sequence (and thus massive) secondaries are required from their optical identifications. These ELMBPs are much less common than the very low mass (secondary) systems, the VLMBPs, with secondary masses usually  $\lesssim 0.05 M_{\odot}$ .

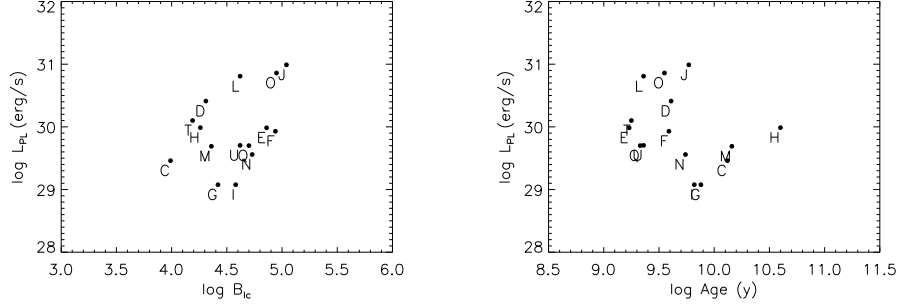


Figure 6. Plot of “PL luminosity” ( $= L_{0.01-8\text{keV}} - L_{NSA}$ ) for each MSP in 47Tuc with measured  $\dot{P}$  using the luminosities for each plotted in the distributions shown in Figure 5b) vs. a) left, magnetic field at the MSP light cylinder and vs. b) right, spindown age,  $P/2\dot{P}$ .

However, some of these VLMBPs are eclipsing (e.g. MSP J, which Camilo et al. (2000) note is eclipsed at 70 cm and 50 cm, but not at 20 cm, for about a quarter of its orbit) and have luminous hard components. A magnetospheric vs. pulsar wind shocked gas origin for the hard component would both likely scale with  $B_{lc}$ .

The magnetospheric vs. shocked gas origin for the “PL” component could be tested by (much) more sensitive spectra which would also distinguish PL from a hot thermal bremsstrahlung component, though brems is surely ruled out by dispersion measure constraints, as pointed out by GCH02. Pulsation analysis would provide a definitive test since the shocked gas origin should not be pulsed due to the emission region having size (much) larger than the characteristic pulse period length scale,  $c \cdot P \sim 10^8$  cm. Unfortunately, detailed spectral fits are not possible with the present Chandra data given the limited statistics, and pulsed profiles vs. energy are not possible with Chandra-ACIS (or Chandra-HRC). Thus we cannot prove the “PL” component is of magnetospheric origin on these old, weak-field MSPs.

Another test can be done, however: plot the hard X-ray luminosity,  $L_x(\text{PL})$ , vs.  $\dot{E}$  and compare with the soft X-ray luminosity  $L_x(\text{NSA})$  vs.  $\dot{E}$  (as in GCH02). If the hard component is magnetospheric, it will likely fall closer onto the roughly linear  $L_x \sim \dot{E}$  relation shown for field MSPs and luminous GC-MSPs (Becker and Trumper 1999, GCH02) than to the  $L_x \sim \dot{E}^{0.5}$  relation for the soft component that is likely due to polar cap heating (GCH02). Using the  $\dot{E}$  values for the 47Tuc MSPs corrected for cluster acceleration (GCH02), we plot  $L_x$  vs.  $\dot{E}$  in Figure 7 for the two components of  $L_x$ . The  $L_x(\text{NSA})$ – $\dot{E}$  relation has slope  $0.3 \pm 0.2$ , which is marginally flatter than the slope  $0.5 \pm 0.2$  relation found in GCH02 for the dependence of the 0.5–2.5 keV luminosity measured with ACIS-I for a mean BB spectrum with  $kT = 0.22$  keV. The  $L_x(\text{PL})$ – $\dot{E}$  relation appears steeper, with slope  $0.6 \pm 0.3$  from fitting all the points. However a slope 1 relation is also consistent and in fact approximately “bisects” and is parallel to the two apparent groups of points (the lower of which is formed by MSPs G, I, N, U, Q, F, E; this grouping can also be seen in Figure 6a).

Thus within the scatter, a linear relation between  $\log(L_x(\text{PL})) - \dot{E}$  is consistent with the data. We suspect the “PL” component lies in a broad band, bounded by the upper and lower groups on either side of the linear correlation line. As suggested above, it is possible that some of these on the more luminous side (e.g. J and O) are a mixture of magnetospheric and shocked gas components. It is thus interesting that MSP O is similar to J in Figure 8, since it is so similar in its binary properties (cf. Figure 5 in Freire, in this volume). Conversely, the “lower group” of MSPs in the  $\log(L_x(\text{PL}))$  vs.  $\dot{E}$  plot are dominated by single MSPs (F, G, N, U), wide binaries (E, Q) or those with extremely low mass companions (I, with  $M_c \sim 0.01 M_\odot$ ; Freire, in this volume).

### 3.3. 47TucW and Total MSP Populations

We have already hinted at the special role MSP W in 47Tuc has assumed. As an eclipsing (3.1h) radio MSP with a main sequence (MS) companion discovered with HST (Edmonds et al. 2002), it is similar in many respects to the 1.3d binary-eclipsing MSP 6397A with MS (or evolved) companion in NCG 6397. As noted in Edmonds et al., the X-ray spectrum derived with the original Chandra ACIS-I observation is also similar: a hard spectrum (fit with a PL with photon index  $\Gamma = 1.8 \pm 0.6$ , with  $L_x(0.5\text{--}2.5 \text{ keV}) = 7.8 \times 10^{30} \text{ erg s}^{-1}$  vs. values  $1.6 \pm 0.3$  and  $4 \times 10^{30} \text{ erg s}^{-1}$  for 6397A.

The deep Chandra observation of 47Tuc has greatly expanded our view of MSP W, with more than  $7\times$  the total number of counts. The X-ray spectrum and variability, as well as the simultaneous HST/ACS-WF data and archival ACS-HRC data, are described in detail in BGvdB04. As included in Figure 5, we now fit W with an NSA model with  $T = 1.03 \times 10^6 \text{ K}$  and radius (at the NS) of 1.4km for a thermal luminosity of  $L_{\text{NSA}} = 7.8 \times 10^{30} \text{ erg s}^{-1}$  and a PL component with photon index  $1.3 \pm 0.25$  and non-thermal luminosity  $L_{\text{PL}} = 2.8 \times 10^{31} \text{ erg s}^{-1}$ . From comparison with the qLMXB J1808.4–3658, we conclude that MSP W is the long-sought missing link between MSPs and qLMXBs in its properties and that it constrains the origin of the hard PL component seen in many qLMXBs to be due to the shocked gas due to an underlying pulsar wind, as recently suggested by Campana et al. (2004) and references therein.

Here we simply comment on the implications for finding an X-ray population of hard (“PL emission”) MSPs, like W, for the total population of MSPs in 47Tuc or in other clusters. Freire (in this volume) notes that there are now 6 such eclipsing MSPs known in GCs (including the three with optically identified MS like companions: 47TucW, 6397A and PSR B1718–19 in NGC 6349; and 3 additional likely candidates in other GCs) out of some 80 total MSPs known in GCs. This of course is based on a radio-selected sample (all MSPs were originally discovered as radio objects). However these objects as well as the EVLMBPs (e.g. J) are all subject to eclipses and variable absorption in the radio. We note that 47TucW was only detected for 4h (Camilo et al. 2000), thus precluding a timing measurement for its apparent  $\dot{P}$  and therefore our including W with a derived  $B_{lc}$  or age in Figure 6 or  $\dot{E}$  in Figure 7. Our Chandra spectra now also indicate that at least two of these (6397A and 47TucW) are similar in their PL-component X-ray spectra, which are likely also due to pulsar wind shocked gas rather than magnetospheric emission in hard X-rays. Thus the Chandra deep images can detect these objects regardless of their radio detectability and

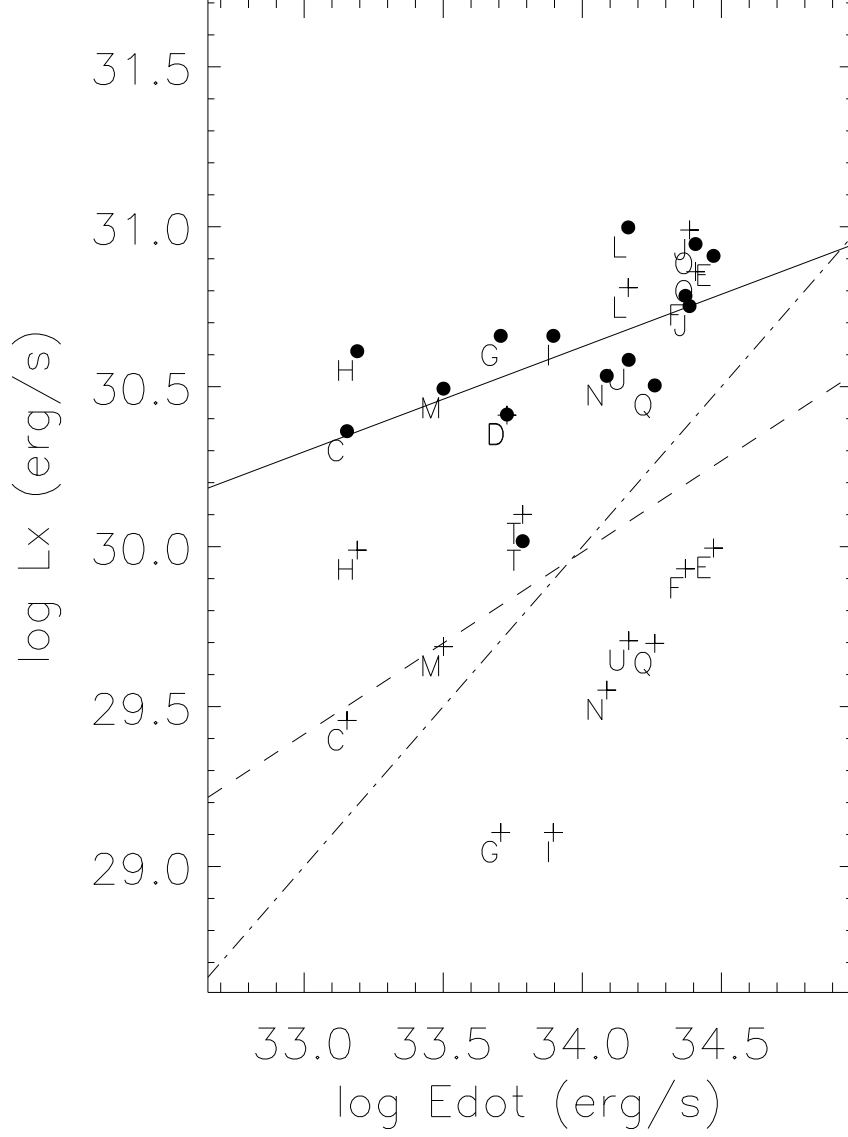


Figure 7. Log-log plot for X-ray luminosity vs. spindown luminosity,  $\dot{E}$ , for thermal (NSA) component ( $\bullet$ ) vs. power law component ( $+$ ). The linear regression lines shown are for the thermal luminosities ( $\log(L_x) = 19.5 \pm 4.6 + 0.33 \pm 0.13 \log(\dot{E})$ , solid line), PL luminosities ( $\log(L_x) = 10.6 \pm 11.7 + 0.57 \pm 0.35 \log(\dot{E})$ , dashed line), and a linear relation for the PL luminosities ( $\log L_x = -4 + \log(\dot{E})$ ), dash-dot line), which bisects the upper and lower tracks of PL points and would be consistent with the linear Becker and Trumper (1999) relation for more luminous pulsars dominated by magnetospheric emission.

inclination; MSP W is dominated by hard emission that would not be eclipsed if the system were at inclination  $i \lesssim 40^\circ$  but in fact is eclipsed for part of the binary orbit since it likely arises from shocked gas near the L1 point (BGvdB04).

This suggests that some of the hard source population in 47Tuc and other GCs could be additional MSPs that are permanently “eclipsed” in radio by the winds driven from their secondary companions by pulsar wind shock heating. Thus the  $\sim 8\%$  fraction of ELMBPs inferred by Freire (in this volume) must be a lower limit; all those that are permanently eclipsed in radio are not counted. These hard X-ray sources would be variable (on binary phase timescales) and could appear as blue objects due to pulsar wind-heated stellar companions or possibly heated accretion streams, prevented from accreting by pulsar winds. We note that heating effects (and moderately blue companions) are only expected for the shortest orbital period systems like W; those which have second-exchange captured companions in to  $\gtrsim 6$ –8h periods (like 6397A, with 1.3d orbital day period) would likely not show heating effects (though  $H\alpha$  may still be detected). As hard sources with otherwise main sequence type optical counterparts, they could then be confused with active binaries or BY Dra systems, which is precisely what happened with our initial identification (Taylor et al. 2001) of the optical counterpart of 6397A before the discovery (D’Amico et al. 2001) of the MSP in NGC 6397 and our identification (Grindlay et al. 2001b) of it as a Chandra source. The total number of MSPs in 47Tuc must then include some of these and be larger than the revised estimate of  $\sim 30$ –60 MSPs and  $\sim 400$  NSs derived by Heinke et al. (2004a) in part from the 8% estimate of Freire (in this volume).

#### 4. Are the MSPs and qLMXBs in 47Tuc Anisotropic?

We note that the spatial distribution of the 15 MSPs in 47Tuc with timing positions originally reported by Freire et al. (2001) as well as that of 47TucS (Freire 2001) and now also 47TucW (Edmonds et al. 2002) are suggestive of anisotropy: all but 4 (E, O, L and M) are on the north side of the cluster center, over a range of position angle (PA) bisectors through the cluster center. Interestingly, all 5 of the qLMXBs in 47Tuc (Heinke et al. 2004b) are on the same (N-NW) side of a bisector through the cluster center as the MSPs. In Figure 8 we show the positions of the 17 MSPs and 5 qLMXBs with precise positions in 47Tuc. The binomial probability of only 4 (MSPs D, E, L and M) of 22 objects that are themselves likely drawn from the same parent distribution (LMXBs) being on the SE side of the cluster center is  $4.2 \times 10^{-4}$ ; this increases to  $2.2 \times 10^{-3}$  for 5 objects (over a wider range of PAs).

The significance of this result is thus only  $\sim 3\sigma$  and of course less if all possible “bisectors” are considered. However, the possible anisotropy direction may be “preferred”: the MSPs (and qLMXBs) are approximately on the side trailing the direction of proper motion (PM) of 47Tuc, which is towards  $PA = 233_{-9}^{+12}^\circ$ , as derived by Odenkirchen et al. (1997) by referencing to Hipparcos data. The a-posteriori binomial probability of the 7 MSPs (and no qLMXBs), namely MSPs Q, D, E, T, G/I and W being “below” the bisector line through the cluster center and perpendicular to the PM vector (double-dot-dash drawn in Figure 8) is 0.026. On the other hand, the more accurate PM vector at  $PA = 250 \pm 2^\circ$  reported by Anderson and King (2003) does not suggest this

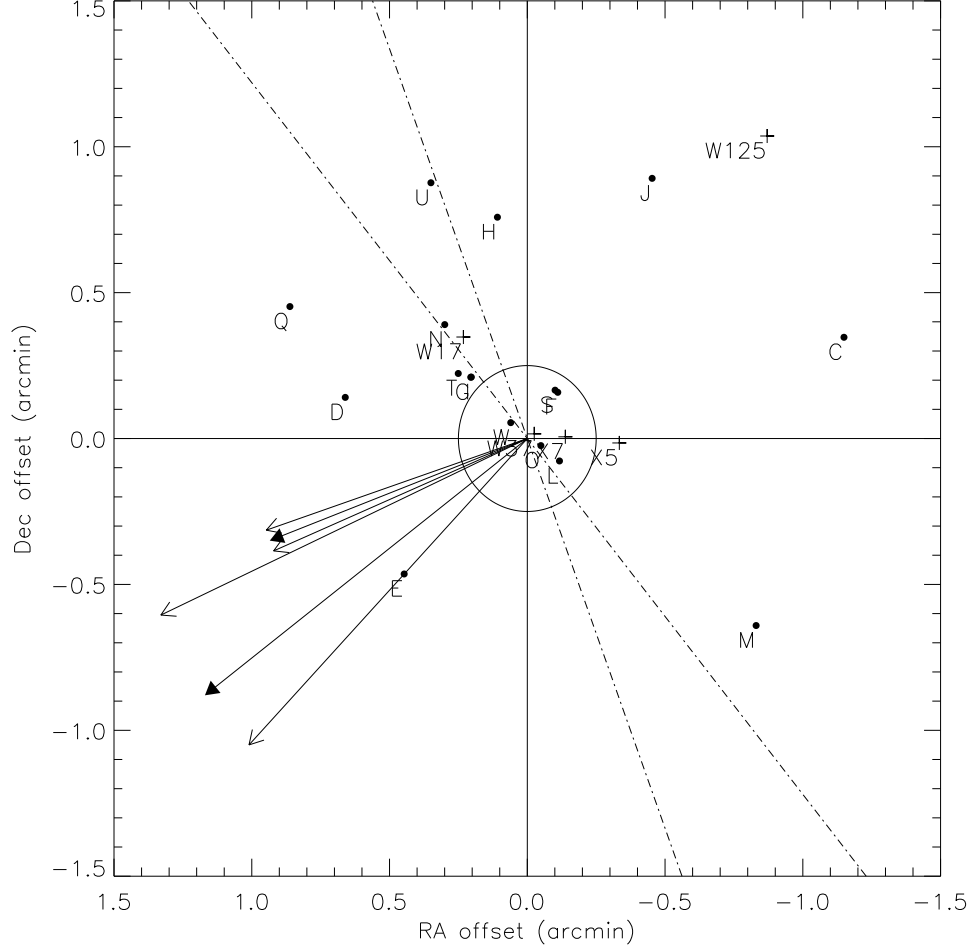


Figure 8. Offsets from the cluster center (de Marchi et al. 1996) of all 17 MSPs ( $\bullet$ ) with known positions and the 5 qLMXBs (+) in 47Tuc compared with the proper motion (PM) vectors and  $\pm 1\sigma$  uncertainties  $250 \pm 2^\circ$  and  $233^{+12}_{-9}^\circ$  of the cluster as reported by Anderson and King (2003) and Odenkirchen et al. (1997), respectively (we show both for comparison since the more accurate value is derived as an offset from the SMC proper motion which may still be subject to systematic uncertainties, though its quoted errors were included). The core radius of the MSPs and qLMXBs in 47Tuc,  $r_c = 15''$  as derived by GCH02, is shown as the circle. The dot-dashed lines are perpendicular to the PM vectors and are similarly uncertain. The Odenkirchen PM vector suggests the MSPs and qLMXBs may be trailing the cluster (7 of 22 are leading); the Anderson-King PM vector suggests they may be offset perpendicular to the cluster motion (7 of 22 are "below" the PM vector). The binomial probabilities for either are about 3% and so only marginally significant (see text).

but instead has a similar number (7) of MSPs (E, O, L, M) and qLMXBs (X7 and X5) offset to one side of the PM vector. This PM determination, while statistically more accurate, is measured relative to the SMC for which the value reported by Irwin (1999) contributes the dominant error and which may still contain systematic effects. Thus, overall, the anisotropy may be associated with the cluster proper motion at the  $\sim 2\sigma$  level.

Regardless of any association with the cluster PM, if the MSP-qLMXB distribution is anisotropic, it is unlikely that selection effects could introduce azimuthal anisotropy in the Chandra source distribution (indeed the overall X-ray source distribution in Figure 1 is isotropic), and no dispersion measure (DM) gradients are present in the DM values given by Freire et al. (2001) that could give rise to a lack of radio detections of MSPs in the SE quadrant. In contrast, the comparable numbers of Chandra sources optically identified by Edmonds et al. (2003a,b) with CVs (22) and active binaries (29), which are chromospherically active main sequence binaries, appear to be isotropic in the deep HST images used for their identification.

Why should the MSPs/qLMXBs, predominantly, be affected by the cluster motion if the trailing or perpendicular associations are significant? We note that if the MSP/qLMXB offsets are real, they would not be expected to show up in the present PM measures for the MSPs (four are given in Freire et al. (2001)) vs. the cluster PM since the difference must be negligible for the MSPs to remain bound to the cluster. As the oldest compact binary population, with (typically) degenerate secondaries, the MSPs (and qLMXBs) may have accumulated the largest net recoil deflections by weak encounters with soft main sequence binaries in the galactic halo and disk. An MSP (or qLMXB) will have weak encounters with wide field binaries (with semi-major axes typically  $a_f = 100\text{AU}$ ) in the disk and galactic halo, which are (much) too soft to survive in the cluster core, at a rate  $R_f \sim n_f \sigma_f v_f$ . Adopting a weak encounter impact parameter as  $b_f \sim 100a_f$ , which would typically Rutherford scatter a cluster MSP to induce a  $\sim 1\%$  velocity perturbation on the typical  $\sim 10 \text{ km s}^{-1}$  velocity of the MSP in the cluster, a field binary density  $n_f \sim 10^{-3} \text{ pc}^{-3}$ , and cluster velocity relative to the field  $v_f \sim 100 \text{ km s}^{-1}$ , the time between such encounters is  $\tau_f = 1/R_f \sim 10^{8-9} \text{ y}$ . This is comparable to the weak encounter time for an MSP with cluster binaries in the core of 47Tuc, which as hard binaries have  $a_c \lesssim 1\text{AU}$ ,  $n_c \sim 10^3 \text{ pc}^{-3}$  (for an assumed 1% binary fraction for such wide binaries in 47Tuc), and relative velocity in the cluster  $v_c \sim 10 \text{ km s}^{-1}$ . These weak encounters will be isotropic in the cluster frame for cluster binary perturbers but anisotropic for field binaries, which will impart (small) recoil momentum transfer to the MSPs and qLMXBs. Since the maximum transfer is at closest approach, it would seem the recoil velocities would be preferentially in the perpendicular direction. Note that such recoils would occur preferentially when the compact binaries are near apastron in their largely radial cluster orbits (where they spend the most time), so that relatively small  $\Delta v$  values imparted to the binary can have the largest effect. The length of the PM arrows are drawn in Figure 8 for the two different PM values and show the approximate motion of the center of mass of the cluster and MSPs over  $10^4$  years. The comparable offsets of the MSPs, if acquired over their  $\sim 10^9$  year lifetimes, thus represent a net drift velocity of only  $\sim 10^{-2} \text{ km s}^{-1}$ , or comparable to the induced velocity perturbation by scattering off field binaries.

Single cluster stars have smaller cross sections than binaries for scattering off field binaries, and without the internal degree of freedom provided by the binding energy of a cluster binary, scattering of single stars are likely perturbed more isotropically by their encounters. Cluster CVs and ABs have binary evolution lifetimes generally (much) shorter than MSPs and may also absorb their recoils in tidal distortion of their non-degenerate secondaries (absent for all the known MSPs in 47Tuc except W). Detailed simulations and a full diffusion analysis are of course needed to test whether disk and halo binary encounters can scatter the orbits of compact binaries in a cluster preferentially and not alter (significantly) their radial distribution (GCH02), which is consistent with an isothermal King profile with core radius  $r_c = 15''$  (cf. Fig. 8) as expected for  $\sim 1.5M_\odot$  objects in dynamical equilibrium with predominantly  $0.7M_\odot$  stars in the core.

Clearly both a larger sample of MSPs and/or qLMXBs is needed to test the reality of this (marginal) anisotropy as well as speculative interpretation. Based on X-ray luminosity and spectral colors and absence of variability or CV/AB optical counterparts, additional MSP candidates in the original ACIS-I data have been given by GCH02 and Edmonds et al. (2003a) but have been reduced by Heinke et al. (2004a) to just 4 or 5 in the ACIS-S data: W5, W28, W34, W142 and possibly W6. All of these additional MSP candidates are again perpendicular (and on one side) of the Anderson-King PM vector but only two (W34 and W142) are on the “trailing” side. This would support the picture of preferentially perpendicular (to the PM vector) scattered velocity perturbations, though it is puzzling these are not symmetrically distributed about both sides rather than just the north side. In addition, of course, there are at least 5 radio MSPs in 47Tuc still not located with radio timing, and as noted above, Heinke et al. (2004a) estimate there are an additional  $\sim 10$ – $40$  additional MSPs likely present in 47Tuc (likely a lower limit; see above). Thus MSP/qLMXB possible anisotropy and diffusion effects will be testable.

## 5. Conclusions

MSPs in GCs remain a treasure to be mined further with high spatial resolution X-ray imaging as well as high throughput spectroscopy. They are low luminosity objects which must be resolved, cleanly, from comparably bright CVs and ABs. It is clear that Chandra and future higher throughput telescopes, with comparable or (ideally) better angular resolution ( $< 1''$ ) are needed. With Chandra, very long observation times are required to make significant new progress on MSPs. Accordingly, we have concentrated here on X-ray spectra derived from our 300ksec observation of 47Tuc and have shown that they are generally all consistent with a combination of soft thermal emission from their polar caps plus a harder PL component. The thermal temperatures (derived for a NSA model) are in a surprisingly narrow range:  $1.1 \pm 0.2 \times 10^6$  K. The “PL component” can only be fitted as such in the four brightest MSPs; for the others we can only say there is an excess of flux above the thermal fits at  $\gtrsim 2$  keV which is consistent with a PL origin.

We note that this hard X-ray component could be either magnetospheric or pulsar-wind shocked gas or both. Shocked gas is certainly the case for the brightest “hard” MSP in 47Tuc, MSP W (BGvdB04). MSPs, generally, may



have all three components – polar cap, magnetospheric and pulsar wind-induced, with the latter most prominent for the doubly-exchanged systems with main sequence companions (47TucW and 6397A).

It is interesting that the luminosities separately derived here for the thermal (NSA or BB) and PL components have correlations with  $\dot{E}$  consistent with log-log slope 0.5 and 1, respectively. The PL component decreases in luminosity with MSP age and field at the light cylinder, both of course due to variations in  $\dot{P}$ . We note again that all  $\dot{P}$  values are the same intrinsic values corrected for the MSP acceleration in the cluster as described in GCH02.

We have called attention to a puzzling, though marginally significant, apparent anisotropy of the MSPs and qLMXBs in 47Tuc: this may (or may not) be associated with the cluster proper motion. Weak encounters the oldest cluster compact binaries, the MSPs and qLMXBs – NSs with (typically) degenerate binary companions – with soft binaries in the field (both halo and disk) may provide an explanation, but detailed simulations are needed and, of course, more MSP/qLMXB precise positions are required to confirm the effect.

X-ray pulse timing and pulse-phased spectroscopy is the obvious new domain which would provide crucial tests. The soft thermal component emission should show up as broad quasi-sinusoidal emission, which can test the polar cap geometry (and presence of multipoles; cf GCH02). The magnetospheric component is beamed (at least partly) and will generally produce narrower pulse profiles dominated by PL emission; whereas the PL component from the pulsar wind and shocked gas from the binary companion will be unpulsed. It is unfortunate that the only pulsar timing capability on Chandra is the HRC-S with its limited sensitivity above 2 keV, high internal background, lack of any spectral sensitivity and limited response above  $\sim 2$  keV. Nevertheless, the 800 ksec HRC-S observation to be conducted in Cycle 6 by Rutledge et al. will make an important start on measuring these predicted components (though the sensitivity for the PL component will be limited) and may enable Chandra identification of the remaining 5 radio MSPs by detecting their soft pulsations from among the ACIS-S sources.

I thank Craig Heinke and Slavko Bogdanov for many discussions and for preparing Figures 1 and 2–4, respectively, and Andrew Lyne for discussions about the puzzling possible MSP anisotropy. This work was supported in part by NASA grants GO2-3059A and HST-GO-09281.01-A.

## References

- Anderson, J. and King, I. 2003, *ApJ*, 126, 772
- Becker, W. et al. 2003, *ApJ*, 594, 798
- Becker, W. and Trumper, J. 1999 *A&A*, 341, 803
- Bogdanov, S., Grindlay, J., and van den Berg, M., *Science*, submitted (BGvdB04)
- Bogdanov, S., Grindlay, J., Heinke, C. et al. 2004, *ApJ*, in preparation (BGH04)
- Camilo, F., Lorimer, D., Freire, P., Lyne, A., Manchester, R. 2000, *ApJ*, 535, 975
- Campana, S. et al. 2004, *ApJ*, in press (astro-ph/0408584)

- D'Amico, N., Lyne, A., Manchester, R., Possenti, A. and Camilo, F. 2001, *ApJ*, 561, L89
- Danner, R., Kulkarni, S.R., Saito, Y. and Kawai, N. 1997, *Nature*, 388, 751
- DeMarchi, G. et al. 1996, *ApJ*, 468, L51
- Edmonds, P., Gilliland, R., Heinke, C., Grindlay, J. and Camilo, F. 2001, *ApJ*, 557, L57
- Edmonds, P., Gilliland, R., Camilo, F., Heinke, C. and Grindlay, J. 2002, *ApJ*, 579, 741
- Edmonds, P., Gilliland, R., Heinke, C. and Grindlay, J. 2003a, *ApJ*, 596, 1177
- Edmonds, P., Gilliland, R., Heinke, C. and Grindlay, J. 2003b, *ApJ*, 596, 1197
- Ferguson, C., Lei, F., Dean, A. J., Bird, A. J., Lockley, J. J. 1999, *A&A*, 350, 847
- Ferraro, F., Possenti, A., D'Amico, N., and Sabbi, E. 2001, *ApJ*, 561, L93
- Freire, P. 2001, Ph.D. Thesis, Manchester University
- Freire, P., Camilo, F., Lorimer, D., Lyne, A. and Manchester, R. 2001, *MNRAS*, 326, 901
- Grindlay, J., Heinke, C., Edmonds, P. and Murray, S. 2001a, *Science*, 292, 2290 (GHE01)
- Grindlay, J., Heinke, C., Edmonds, P., Murray, S. and Cool, A. 2001b, *ApJ*, 563, L53
- Grindlay, J., Camilo, F., Heinke, C., Edmonds, P., Cohn, H. and Lugger, P. 2002, *ApJ*, 581, 470 (GCH02)
- Heinke, C. et al. 2004a, *ApJ*, submitted
- Heinke, C. et al. 2004b, *ApJ*, submitted
- Irwin, M. 1999, in *IAU Symp. 192, the Stellar Content of Local Group Galaxies*, ed. P. Whitelock & R. Cannon (San Francisco: ASP), 409
- Kawai, N. and Saito, Y. 1999, *Astrophys. Lett. Commun.*, 38, 1
- Kuiper, L., Hermsen, W., Verbunt, F. and Belloni, T. 1998, *A&A*, 336, 545
- Lloyd, D. 2003, *astro-ph/0303561*
- Odenkirchen, M., Brosche, P., Geffert, M. and Tucholke, H. 1997, *New Astron.*, 2, 477
- Taylor, J., Grindlay, J., Edmonds, P. and Cool, A. 2001, *ApJ*, 553, L169
- Webb, N., Olive, J. and Barret, D. 2004, *A&A*, 417, 181
- Zavlin, V., Pavlov, G., et al. 2002, *ApJ*, 569, 894
- Zhang, L. and Cheng, K. 2003, *A&A*, 398, 639